Pharm Res (2011) 28:2931–2944
DOI 10.1007/s11095-011-0561-z

RESEARCH PAPER

# Gold Nanoparticle Penetration and Reduced Metabolism in Human Skin by Toluene

Hagar I. Labouta • David C. Liu • Lynlee L. Lin • Margaret K. Butler • Jeffrey E. Grice • Anthony P. Raphael • Tobias Kraus • Labiba K. El-Khordagui • H. Peter Soyer • Michael S. Roberts • Marc Schneider • Tarl W. Prow

Received: 23 April 2011 / Accepted: 3 August 2011 / Published online: 11 August 2011


## ABSTRACT

***Purpose*** To measure penetration and metabolic effects of ion-stabilized, polar, 15 nm gold nanoparticles in aqueous solution (AuNP-Aq) and sterically stabilized, non-polar, 6 nm gold nanoparticles in toluene (AuNP-TOL) on excised human skin.

***Methods*** Gold nanoparticles were characterized with dynamic light scattering and transmission electron microscopy (TEM). Skin penetration studies were done on frozen or fresh excised skin using static Franz diffusion cells. Viable treated skin was assessed by dermoscopy, reflectance confocal microscopy (RCM), multiphoton tomography (MPT) with fluorescence lifetime imaging microscopy (FLIM), and TEM.

***Results*** Dermoscopy and RCM showed large aggregates in the furrows of AuNP-Aq-treated skin. Treatment of thawed and viable skin only showed enhanced permeability to nanoparticles in the AuNP-TOL group with MPT and FLIM imaging to stratum spinosum of epidermis. TEM analysis revealed gold nanoparticles within AuNP-treated stratum corneum. FLIM analysis of NAD(P)H showed a significant decrease in total NAD(P)H in all toluene-treated groups.

***Conclusions*** Gold nanoparticles, 15 nm, in aqueous solution aggregated on the skin surface. Toluene treatment eliminated skin metabolism; skin treated with toluene/gold nanoparticles (6 nm) for 24 h, but not at 4 h, showed increased nanoparticle permeability. These results are of value to nanotoxicology.

**KEY WORDS** confocal reflectance microscopy · fluorescence lifetime · multiphoton microscopy · nanoparticle · skin

## ABBREVIATIONS

| | |
|---|---|
| ANOVA | analysis of variance |
| AuNP | gold nanoparticle |
| AuNP-Aq | gold nanoparticle in aqueous solution |
| AuNP-TOL | gold nanoparticle in toluene |
| BP | band pass filter |
| EDXS | energy-dispersed X-ray spectroscopy |

Hagar I. Labouta and David C. Liu contributed equally to this work.

H. I. Labouta · M. Schneider (✉)
Department of Pharmaceutical Nanotechnology, Saarland University
Saarbrücken, Germany
e-mail: Marc.Schneider@mx.uni-saarland.de

H. I. Labouta · L. K. El-Khordagui
Department of Pharmaceutics, Alexandria University
Alexandria, Egypt

D. C. Liu · L. L. Lin · J. E. Grice · A. P. Raphael · M. S. Roberts · T. W. Prow
Therapeutics Research Unit, The University of Queensland
Brisbane, Australia

L. L. Lin · A. P. Raphael · H. P. Soyer · T. W. Prow (✉)
Dermatology Research Centre, School of Medicine
The University of Queensland, Princess Alexandra Hospital
Brisbane, Australia
e-mail: t.prow@uq.edu.au

M. K. Butler · A. P. Raphael
Australian Institute for Bioengineering and Nanotechnology
The University of Queensland
Brisbane, Australia

M. K. Butler
Australian Microscopy and Microanalysis Research Facility
The University of Queensland
Brisbane, Australia

T. Kraus
Structure Formation Group INM Institute
Saarbrücken, Germany

M. S. Roberts
School of Pharmacy and Medical Science
The University of South Australia
Adelaide, Australia

| | |
|---|---|
| FLIM | fluorescence lifetime imaging microscopy |
| HFT KP | dichroic low pass filter |
| ICP | inductively coupled plasma |
| MPT | multiphoton tomography |
| MPT-FLIM | multiphoton tomography with fluorescence lifetime imaging microscopy |
| NA | numerical aperture |
| NAD(P)H | nicotinamide adenine dinucleotide and nicotinamide adenine dinucleotide phosphate |
| RCM | reflectance confocal microscopy |
| SB | stratum basale |
| SC | stratum corneum |
| SG | stratum granulosum |
| SS | stratum spinosum |
| TEM | transmission electron microscopy |
| TEWL | trans-epidermal water loss |
| VE | viable epidermis |

## INTRODUCTION

Penetration and adverse effects of topical nanoparticle exposure is an important issue for public health, regulatory agencies, and industry (1–3). Our skin is exposed to a number of nanoparticles from natural and manmade sources. Nanoparticulates, such as zinc oxide and titanium oxide, are useful sunscreens found in cosmetics. The penetration and nanotoxicology in skin is a debated topic in academia, from small interest groups and regulatory agencies (4,5). The capacity of nanoparticles to overcome the stratum corneum and reach the viable skin is dependent on the model, barrier integrity, nanoparticle (size, shape, surface properties, and charge) and nanoparticle degradation kinetics (1,6,7). Tape stripping (8), mechanical flexion (9), UV exposure (10), sonophoresis (11), and microneedles (12) have all been shown to increase nanoparticle penetration in skin. However, there is a gap in the literature with regard to nanoparticle studies done in human skin with a focus on workplace exposure. Yet, there are several toxicity studies based on cell-culture experiments as well as skin penetration studies to evaluate the safety of topical application of nanoparticles. These studies were previously reviewed by Crosera *et al.* (13), Cevc and Vierl (14), Prow *et al.* (15), Schneider *et al.* (3), and others.

Nanoparticle skin exposure can come from topical products, but, importantly, workplace exposure is a critical area of nanotoxicology without a significant knowledge base (6,16,17). Solvents are commonly used in the workplace (18) and in the synthesis of nanomaterials (19). While solvent effects on drug penetration kinetics have been studied extensively (20,21), very few studies exist on penetration and toxic effects of solvent/nanoparticle in topical exposure scenarios (17). Beyond the workplace, separating solvent and nanoparticle effects is critical for estimating toxicity. One example is the case of colloidal fullerene nanoparticles reported to be toxic in a variety of tests, where the toxicity is now being attributed to the solvent, tetrahydrofuran, and not the nanoparticle (22). We hypothesised that gold nanoparticles could serve as model nanoparticles for examining the combined effects of topical nanoparticles and solvents. This is the first report to simultaneously quantify nanoparticle penetration and metabolic effects of toluene and nanoparticles in human skin.

Xia *et al.* (2010) reported on the penetration of small fullerene nanoparticles, 1 nm, in four solvents—toluene, cyclohexane, chloroform, and mineral oil—on Yorkshire weanling pigs (17). Chloroform, cyclohexane, and toluene increased nanoparticle penetration into deeper layers of the stratum corneum. Toluene was the second solvent after chloroform promoting fullerene penetration into stratum corneum. Xia *et al.* proposed that the mechanism of action was not wholly due to the solubility of the nanoparticle in the solvent. Further, two other mechanisms were proposed including solvent flux and solvent evaporation-induced supersaturation (17). Our goal was to evaluate the solvent and nanoparticle combination. We chose gold nanoparticles as a model nanoparticle because of the inert nature of gold and the capacity to track these particles by two-photon luminescence (23,24).

Noble metal photoluminescence was described in 1969 (1) and two-photon luminescence reported in 1986 (25). The optical and photonic properties of gold nanoparticles are favourable for biomedical imaging, in part because of enhanced light absorption to $1.4\times10^{7}$ and $3.7\times10^{8}$ $M^{-1}cm^{-1}$ for 5 nm and 15 nm particles, respectively. However, the body of literature in the field of dermatology is limited with regard to topical gold nanoparticle application. There are several reports on gold nanoparticle effects on cultures of skin-derived cell lines (26–28). However, there are no reports on the metabolic consequences of topical gold nanoparticle application on skin or any reports measuring penetration depth of nanoparticles less than 12 nm in human skin. Sonavane *et al.* (2008), showed penetration of 15 nm gold nanoparticles through excised rat skin after 24 h. These data show that there is potential for small gold nanoparticles to penetrate deep enough through skin to reach the circulatory system in the dermis; thus, there may be some risk of systemic nanoparticle exposure. A recent report by Larese Filon *et al.* (2011) supports the earlier findings of Sonavane. They found similar results when evaluating gold nanoparticle penetration (12.9 nm) in thawed human skin (29). Gold nanoparticles were detected in the receiving solution of the Franz cells after 24 h of skin exposure. The authors also investigated the effects of skin abrasion on gold nanoparticle penetration.

The objectives of this study include an in-depth investigation of the consequences of topical exposure to two gold nanoparticle formulations, with different size, charge, surface chemistry, and vehicle, in terms of penetration and metabolic changes in human skin using multiphoton tomography (MPT), TEM, reflectance confocal microscopy (RCM), dermoscopy, and fluorescence lifetime imaging microscopy (FLIM). Our data suggest that toluene, a common industrial solvent, is associated with increased nanoparticle penetration through viable human skin, but only after long-term exposure.

## MATERIALS AND METHODS

### AuNP-Aq Synthesis

Ionically-stabilised polar AuNP were prepared using the Turkevitch method (30). A 100 μg/ml solution of hydrogen tetrachloroaurate (70 ml, $HAuCl_4 \cdot 3\ H_2O$, Sigma-Aldrich Chemie GmbH, Steinheim, Germany) was heated to 100°C under stirring at 440 rpm and then reduced by adding a solution of trisodium citrate dihydrate ($Na_3C_6H_5O_7 \cdot 2\ H_2O$, Sigma-Aldrich) containing 5-fold molar concentration of gold salt. After the gold colloid had formed, the temperature was lowered to 25°C. The colloid was then stored at 4°C in the dark.

### AuNP-TOL Synthesis

Sterically stabilised apolar AuNP were synthesised as described by Zheng *et al.* (31). AuNP were formed upon gold reduction by an amine-borane complex in the presence of an alkyl thiol. In a typical synthesis, 0.31 g chlorotriphenylphosphine gold (purity 98%, ABCR, Karlsruhe, Germany) was dissolved in 50 ml of benzene (purity >99.5%, Riedel-de Haen, Germany), forming a colorless solution. A mixture of 0.53 g tert-butylamineborane (purity, 97%, Fluka, Germany) and 0.31 ml dodecanethiol (purity >98%, Fluka, Germany) was added to the formed solution and left to react at 55°C for 1 h. Upon completion of the reduction reaction, the red solution was cooled to room temperature, precipitated by the addition of ethanol and washed by centrifugation and subsequent resuspension in toluene. Finally, the resuspended particles were stored at room temperature away from light.

### Nanoparticle Characterisation

The optical properties of the AuNP were recorded using a UV/Vis spectrophotometer (lambda 35, Perkin Elmer LAS, Germany) in the range of 400–800 nm. Mean particle size of the gold core ($n=30$) and morphology were determined by transmission electron microscopy (TEM) using a JOEL Model JEM 2010 instrument (JOEL GmbH, Eching, Germany) operated at an accelerating voltage of 120 kV. Samples for TEM analysis were prepared by placing 12 μl of dispersed nanoparticles on carbon-coated 400 mesh copper grids. The solvent was allowed to evaporate at room temperature. The nanoparticle hydrodynamic radius was measured using a Malvern Zetasizer Nano (Malvern Instruments, Malvern, UK) based on dynamic light scattering at 25°C. The surface charge of AuNP-Aq was estimated by measuring the zeta potential based on the electrophoretic mobility (Zetasizer Nano, Malvern Instruments, Malvern, UK) in water. The samples (1.5 ml) were run in triplicate using disposable folded capillary cells that contained the electrodes.

### Excised Human Skin Preparation

Human skin was obtained from abdominoplasty patients with the approval of either the Research Ethic Committee of Saarland, Germany (Ärztekammer des Saarlandes, Dec. 2008) (thawed skin experiments) or Princess Alexandra Hospital Research Ethics Committee (No. 1997/097), Australia (viable skin experiments). All volunteers had previously signed informed consent forms. Eleven skin donors were used in this study. The subcutaneous fatty tissue was immediately removed from the skin. The surface of each specimen was cleaned with water. For thawed skin experiments, skin specimens were wrapped in aluminium foil and stored in polyethylene bags at 4°C or −26°C for less than 6 months before further usage. Previous investigations have shown that there is no change in the penetration characteristics of drugs through thawed skin stored frozen for 6 months (32).

Skin discs, 25 mm in diameter, were cut, thawed, cleaned with deionised water/Ringer solution, and transferred into the Franz diffusion cells. Transepidermal water loss (TEWL) was measured with a Biox AquaFlux Condenser Chamber unit (model AF200) to assess barrier integrity before and after 24 h treatment.

### Skin Penetration Studies

*Ex vivo* penetration experiments were carried out in static Franz diffusion cells with previously frozen and viable skin. Skin was mounted in Franz cells with a diffusion area of 1.8 $cm^2$ and 1.1 $cm^2$ and receptor compartment volumes of 12 ml and 3.2 ml volume for frozen and viable skin experiments, respectively. Receptor solution was phosphate-buffered saline, pH 7.4, magnetically stirred at 500 rpm. Nanoparticle-containing solutions in their original dispersion medium, 500 μl at 90 μg/ml, were topically applied in the donor cell. Diffusion cells were maintained at 32°C throughout the 4 and 24 h exposure experiments. Following treatment, the excess nanoparticle solution was drained, and the skin was removed.

### Cryosectioning

Skin was fixed, embedded, and sectioned as previously described (2). Skin was fixed in 2% paraformaldehyde in 0.1 M phosphate buffer pH 7.4 for 2 h at room temperature. Skin sections (10–50 μm thick) were cut at −20°C using a Frigocut 2800 cryostat (Reichert-Jung, Leica, Wetzlar, Germany) or Leica CM1850 cryostat (Leica microsystems, Heidelberger, Nussloch, Germany). The sections were mounted in Prolong Gold (Invitrogen, Mulgrave, Victoria, Australia) or FluorSave™ (Calbiochem, San Diego, USA) prior to microscopic analysis. On cryosectioning, placement of the skin punch was not parallel to the cutting blade of the cryotome to avoid dislocation of the particles from outside into the deeper skin layers or vice versa, but in a perpendicular position limiting sectioning artifacts (24).

### Dermoscopy and Reflectance Confocal Microscopy (RCM)

Treated skin was visualised using RCM (Vivascope 1500, Lucid Inc., Henrietta, NY) with an in-built dermascope used for visualisation of treated skin surface and localisation of nanoparticle aggregates on and within skin. Color dermoscopy images were taken to $6\times6$ mm$^2$ at $1000\times1000$px$^2$. RCM carried out at 830 nm with an optical power between the range of 3–6.9 mW was used to take $500\times500$ μm images at 30X magnification. A z-stack was taken with images taken every 2 μm from the skin surface to a depth of 100 μm. ImageJ (National Institutes of Health, Bethesda, Washington, D.C., USA) was used to analyse the mean intensity of AuNP in the stratum corneum of furrow depth using a threshold of 240–255 to identify highly reflective areas and to render RCM images in 3D.

### Thawed Skin MPT

MPT imaging was performed using an inverted confocal/two-photon excitation fluorescence microscope (Zeiss LSM 510 META system, Carl Zeiss, Jena, Germany), equipped with a Chameleon infrared laser ($\lambda=710$–930 nm). The objective was a water immersion lens 63X NA=1.2; an excitation wavelength of 800 nm, dichroic beam splitters HFT KP 700/488 nm, and an emission filter BP 560–615 nm filter were used. Transmission light images of the skin sections were also taken simultaneously and shown as overlays with the nanoparticle luminescence. Z-stacks were taken with steps every 1 μm until there was no detectable signal. An excitation radiation with transmission energy of 0.6 and 0.5 mW was used for skin and nanoparticle tracks, respectively.

### Viable Skin MPT and FLIM

A multiphoton tomograph (DermaInspect®, JenLab GmbH, Jena, Germany) equipped with a time-correlated single photon counting detectors, FLIM system (Becker and Hickl, Berlin, Germany) was used to simultaneously image nanoparticles and endogenous NAD(P)H as described previously (15). A tuneable laser (Mai Tai, Spectra physics, Mountain View, USA) with a range of 710–920 nm was used as the excitation source and ultra-short pulse width (65 fs) in pulsed mode-locked at 80 MHz. Treated skin was optically sectioned using MPT-FLIM with a 740 nm excitation wavelength from stratum corneum to stratum basale in 5 μm increments using 40X objective lens with an image size of $210\times210$ μm$^2$. The emission was filtered with a 350–650 nm band pass filter (BG39), a <700 nm short pass optical filter, and a 350–450 nm band pass filter. A constant excitation power of 30 mW at the rear of the objective was used. At least three biological replicates were analysed at 4 and 24 h of treatment for each group.

Resulting FLIM data were analysed with SPC 830 2.9 Image software (Becker and Hickl) to generate fluorescence lifetime decay and photon contribution curves from NAD(P)H autofluorescence and gold luminescence. The instrument response function of each FLIM image was calibrated to a sucrose crystal standard (Ajax Finechem Pty Ltd.). The fluorescence decay curve was fitted with a double-exponential model, $N(t)=\alpha_1 e^{-t/\tau_1}+\alpha_2 e^{-t/\tau_2}$, that defines the short and long lifetime/amplitude values. NAD(P)H-related metabolic rate and gold nanoparticle luminescence were quantified as previously described (7,33). NAD(P)H autofluorescence was isolated using $\alpha_1$% from 45–85, and AuNP luminescence was isolated from NAD(P)H using $\alpha_1$% from 90–100. The $\alpha_1$% is the proportion of the emission photons that return to the detector during the short lifetime phase of the decay curve, and the $\alpha_2$% represents the proportion of long lifetime photons. Although fluorescence lifetime changes with changes in the microenvironment, the $\alpha_1$% does not. This allows the AuNP luminescence positive pixels to be separated from skin autofluorescence.

### Transmission Electron Microscopy

A high resolution TEM microscope, fitted with EDXS and selected area electron diffraction, was used to visualize AuNP in treated skin samples. High pressure freezing was used to preserve the skin ultrastructure using a Leica EM PACT2 system. Skin was placed in a $1.5\times0.2$ mm well with a membrane carrier coated with 1-hexadecene and filled with 1-hexadecene and then rapidly frozen. Samples were then stored in liquid nitrogen and transferred to vials

containing 1% osmium tetroxide ($OsO_4$), 0.5% uranyl acetate, and 5% $H_2O$ in acetone. Samples were then cryosubstituted at −85°C for two days before being gradually warmed to room temperature. After cryosubstitution, the sample was removed from the membrane carrier, washed in acetone, and infiltrated in Epon resin with the use of a microwave (3×40 s, 250 W, no vacuum). Infiltration was gradually carried out with Epon in steps of 1:3, 1:2, 1:1, 2:1, 3:1, 100% and 100% Epon:acetone steps (2×3 min, 250 W, vacuum) using a microwave (Biowave, Pelco) at 60°C. Ultrathin sections (60 nm thickness) were cut from the polymerised block, collected on Formvar-coated 200 mesh copper grids, and examined using a JOEL 2010 transmission electron microscope with 80 kV power.

### Statistical Analysis

Differences in measured macroscopic parameters of treated and control groups were tested applying the non-parametric Mann-Whitney *t*-test. Two-way ANOVA analysis was used to determine significance within multiple groups. Level of significance was accepted at $p \leq 0.05$.

## RESULTS

### Characterisation of AuNP

Dynamic light scattering was used to assess physical properties of two nanoparticles formulations (Table I). Both nanoparticles were monodisperse as shown by TEM. Nanoparticle diameters were confirmed with TEM (Fig. 1). Zeta potential measurements showed that the AuNP-Aq were negatively charged and the AuNP-TOL were uncharged. Both prepared AuNP dispersions showed physical stability and no aggregation. Aggregation of gold nanoparticles would be indicated by a large red-shift of the spectral peak and/or strong peak broadening (34).

### Excised Human Skin Barrier Integrity

Transepidermal water loss was used as an indicator of barrier integrity. After receipt, skin was cut into circular pieces and mounted in Franz cells. We then evaluated TEWL in specimens before and after 24 h of treatment. The mean ± SE of TEWL was 26±1, 25±1, 25±2 and 27±1 g/($m^2$h) for the aqueous, toluene, AuNP-Aq, and AuNP-TOL groups before treatment. After 24 h, TEWL had increased to double for all groups. There was no statistical significance between any two groups within a single time point, and there was significant TEWL increase in all groups after 24 h treatment to $p<0.0001$.

### Dermoscopy of AuNP-Treated Skin

After 24 h treatment, skin surface of AuNP-treated and vehicle-only skin samples as visualised using dermoscopy (Fig. 2a–d). Fine purple lines corresponding to the furrows can be seen in AuNP-treated skin (Fig. 2c–d). The color is reminiscent of gold nanoparticle aggregates. There was more intense and bluer color associated with the AuNP-Aq-treated skin compared to the AuNP-TOL group, pointing towards increased aggregation with the aqueous-formulated AuNP.

### RCM of AuNP-Treated Skin

The resolution of RCM enables visualization of cellular morphology and large, reflective nanoparticle aggregates (7). Treated skin was imaged with RCM after 24 h treatment. With RCM we observed distinct morphological changes that suggested toxicity in toluene-treated skin (Fig. 2f, h) but not in skin treated with aqueous dispersions (Fig. 2e, g). Highly reflective aggregates were seen in both nanoparticle treated groups (Fig. 2g, h) but not in vehicle-only controls (Fig. 2e, f). Aggregates were most prominent in the AuNP-Aq group, supporting the hypothesis that the AuNP-Aq were highly aggregated on the skin surface (Fig. 2c, g). As in the dermoscopy images, there were fewer AuNP-TOL aggregates than observed in the AuNP-Aq group (Fig. 2g, h). Aggregates were only observed on and within the upper stratum corneum in nanoparticle-treated groups.

The dermoscopy and *en face* RCM images showed that there were gold nanoparticle aggregates within the skin furrows. A 3D reconstruction of the RCM z-stacks confirmed the presence of large aggregates within the furrows of AuNP-Aq-treated groups and the absence of these aggregates in all other groups (Fig. 3). Figure 3 shows treated skin from a cross-sectional point of view. The dotted line highlights the surface of the skin; the arrowhead in Fig. 3b indicates a representative cluster deep within a furrow.

**Table I** Characteristics of the Prepared AuNP Dispersion

| AuNP-code | Surface chemistry | Size of gold core, nm | DLS radius, nm | Zeta potential, mV | Vehicle |
|---|---|---|---|---|---|
| AuNP-Aq | Citrate ions | 14.9±1.8 | 15.3±0.7 | −35.1±1.9 | Water |
| AuNP-TOL | Dodecanethiol | 6.0±0.8 | 7.2±0.9 | Uncharged | Toluene |

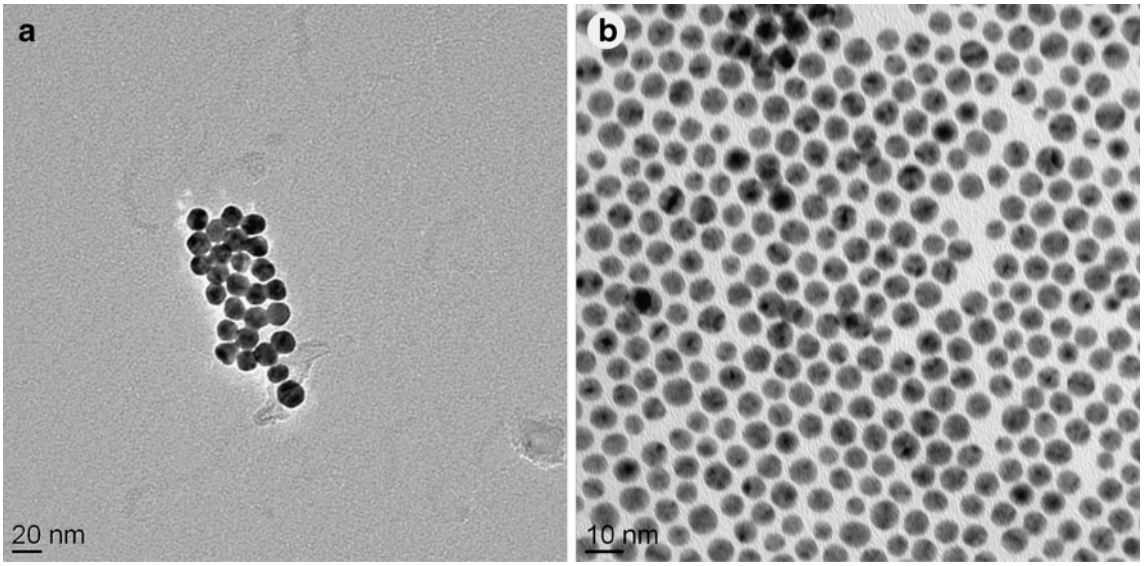


**Fig. 1** (**a**) Citrate-stabilised AuNP-Aq and (**b**) thiol-coated AuNP-TOL imaged with TEM.

### *En Face* MPT-FLIM Analysis of Viable Skin Treated for 4 and 24 Hours

The fluorescence lifetime decay curve contains a short and a long component in this context. The short component represents the photons that return to the detectors quickly, i.e. in the ultrafast multiphoton excited photoluminescence that results from metal nanoparticles and second harmonic generation from collagen. The lifetime is usually reported in picosecond or nanosecond units. Fluorescence lifetimes can change with the microenvironment and are thus not optimal for separating AuNP and NAD(P)H. The α% is the proportion of photons that have short or long lifetimes; this proportion does not change with changes in the microenvironment or concentration. Therefore, we use α% ranges to separate AuNP and NAD(P)H, where intensity changes represent changes in concentration. Skin treated for 4 and 24 h was subjected to MPT-FLIM analysis. The images shown in Fig. 2i–p are from the stratum granulosum layer and are pseudocolored at $\alpha_1$% 50–100% (blue to red). The autofluorescent components of living skin, i.e. NAD(P)H and keratin, can be seen in Fig. 2i, m, k, o in green and blue. Gold nanoparticle luminescence is shown in orange to red in Fig. 2k, l, o, p. Gold nanoparticle signal can be seen primarily in the furrows of nanoparticle-treated skin. Skin treated with aqueous formulations shows clear keratinocyte morphology due to NAD(P)H, found primarily in active mitochondria. Toluene-treated skin shows an absence of NAD(P)H autofluorescence. Skin treated for 24 h with AuNP-TOL revealed AuNP signals from the stratum granulosum suggesting some nanoparticle penetration. This phenomenon was not observed in any other group.

### Cross-Section Analysis of Nanoparticle Penetration with TEM, MPT, and MPT-FLIM

Frozen sections of thawed skin treated with nanoparticle formulations for 24 h showed gold nanoparticle luminescence within the epidermis in AuNP-TOL but not in AuNP-Aq treated samples (Fig. 4). We then used TEM to assess nanoparticle penetration and tissue ultrastructure in viable human skin. Skin treated for 24 h was subject to high pressure freezing for TEM or cryopreservation for MPT-FLIM (Fig. 5). TEM imaging showed ultrastructure indications of toxicity in toluene-treated skin. Stratum corneum showed some delamination, but there were significant signs of toxicity in the viable epidermis. Cell membranes were severely disrupted, including mitochondria and cell junctions (Fig. 5b, d). The electron-dense nature of gold nanoparticles results in increased electron scattering of the incident electrons and thus appears as dark spots in TEM images. Gold nanoparticles were found on the skin surface and up to two cell layers deep in stratum corneum of AuNP-Aq-treated skin (Fig. 5g). Gold nanoparticles were found up to ten cell layers deep in the AuNP-TOL-treated skin, but could not be identified within the viable epidermal layers. This may be due to increased particulate background from the staining solution binding to particulates associated with toluene-damaged tissue (Fig. 5c, d).

Quantification of multiphoton images was conducted. Representative optical z-stacks, 1 μm nominal step width, for examined thawed skin cross-sections were then quantified, according to a method we developed and recently published elsewhere (24). Briefly, the method of quantification is based on calculation of ∑pixel frequency due to AuNP in the SC and DSL, from which weighed number of

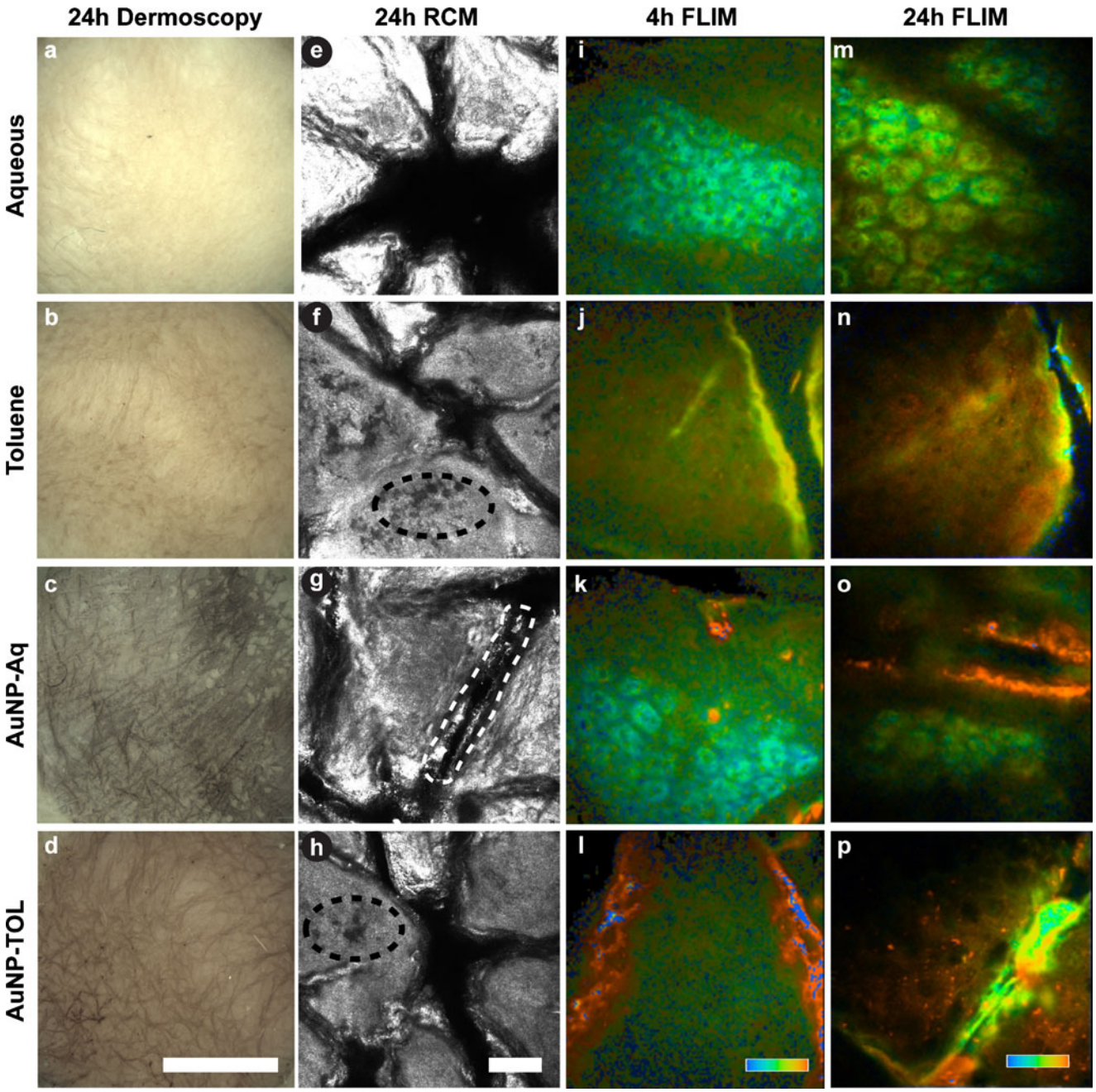


**Fig. 2** Dermoscopy, RCM and MPT-FLIM images of treated human skin. Dermoscopy and RCM images showing the surface of skin specimens treated with aqueous solution, toluene, AuNP-Aq, and AuNP-TOL for 24 h for dermoscopy (**a**–**d**) and for RCM images (**e**–**h**). Black dashed line indicates abnormal reflectance structure within the toluene treated skin (**f**, **h**); white dashed line shows highly reflective particles on the surface of the skin (**g**). FLIM images from the stratum granulosum layer of the epidermis from skin treated for 4 (**i–l**) and 24 h (**m**–**p**). Scale bars: 4 mm (**d**); 50 $\mu$m (**h**, **l**, **p**); pseudocolored MPT-FLIM images are $\alpha_1$% 50–100 from blue to red. Blue-green coloration indicates cellular autofluorescence, i.e. NAD(P)H, and gold nanoparticle luminescence is orange to red (**k**, **l**, **o**, **p**).

particles were calculated. No particles were quantified in DSL of thawed skin specimens treated with AuNP-Aq. On the other hand, results showed depth-profile for AuNP-TOL having higher numbers of AuNP in the upper skin layer, SC (1082 nanoparticles) rather than viable epidermis (470 nanoparticles) (24).

We used MPT-FLIM to separate cellular autofluorescence from gold nanoparticle luminescence. In Fig. 5i, j, cryosections of treated skin are shown with MPT-FLIM and are pseudocolored from blue to red for $\alpha_1$% 50–100%. Cellular autofluorescence is shown in green to yellow; gold nanoparticle luminescence is shown in orange to red. These

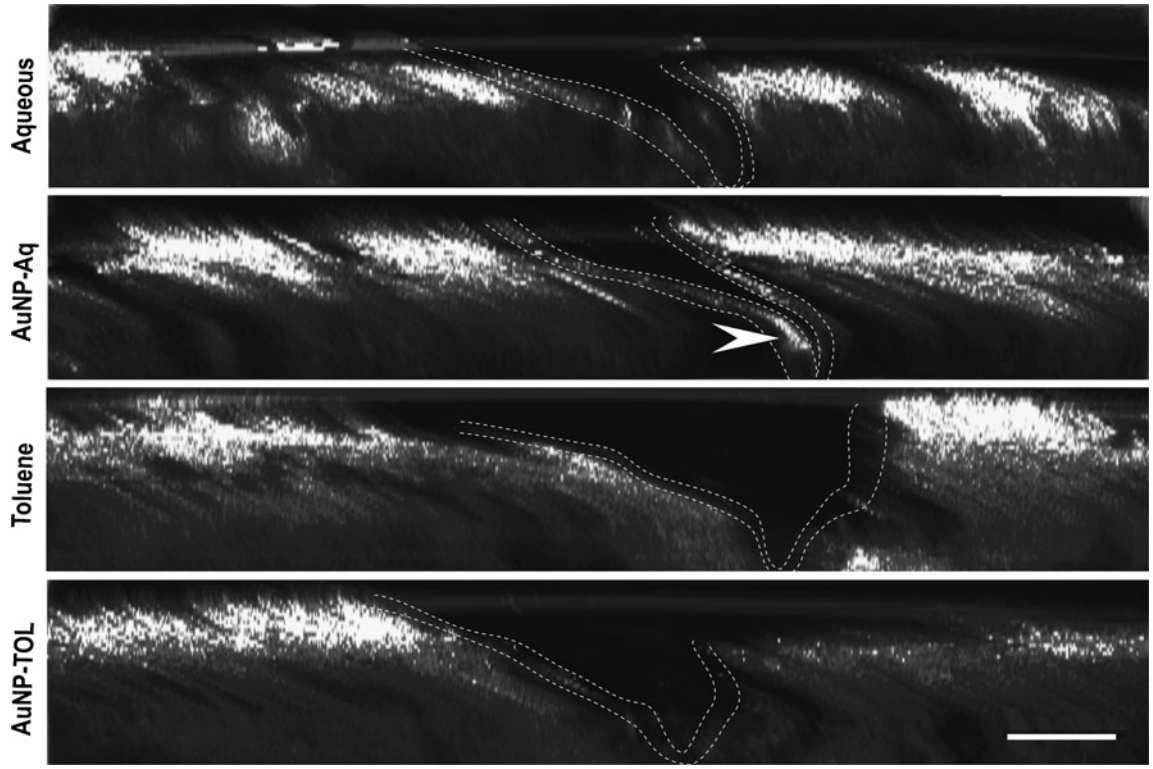


**Fig. 3** 3D reconstructed RCM images rendered in cross section. 3D reconstructed RCM images of skin specimens treated with aqueous solution, AuNP-Aq, toluene and AuNP-TOL. The stratum corneum within the furrows is highlighted with dotted lines. The arrowhead indicates gold nanoparticle aggregates deep within the furrow. Scale bar: 50 $\mu$m.

colors correspond to relatively slow autofluorescence lifetime and relatively instantaneous nature of gold nanoparticle luminescence. Images are oriented so the stratum corneum is at the top and dermis is towards the bottom. Aqueous-treated samples (Fig. 5i, j) show an even green signal through the viable epidermis with dark ellipsoids suggestive of nuclei in position, size, and absence of NAD(P)H signals. These morphological queues are not prominent in toluene-treated skin (Fig. 5k, l), suggesting a lack of the usual membranes that partition NAD(P)H out of the nucleus. The orange signal at the bottom of Fig. 5j, k is likely to be collagen second harmonic generation, where the green-orange interface is the dermal epidermal junction. The second harmonic signal from collagen has overlapping lifetime characteristics with gold luminescence, resulting in an indistinguishable lifetime signature that limits identifying gold nanoparticle signals to the epidermis. Only gold nanoparticle-treated groups show strong signals at the skin surface (Fig. 5k, l). The key difference between the AuNP-Aq and AuNP-TOL images was the presence of punctuate gold nanoparticle signals with a depth-dependent decrease in number from within the viable epidermis in the AuNP-TOL (Fig. 5l), but not in the AuNP-Aq-treated skin (Fig. 5j). These data indicate that gold nanoparticles penetrated deeper within human skin in presence of toluene for 24 h. Importantly, these images were taken from the centre of thick (50 µm) cryosections to minimize potential edge contamination effects, and the punctuate signal pattern was not observed in any of the other treatment groups, including toluene-only control.

### *En Face* MPT-FLIM Intensity Measurement of Gold Nanoparticle Luminescence in Human Skin

Penetration profiles of gold nanoparticle luminescence signals are shown for 4 and 24 h treatment groups in Fig. 6a, b. Depth stacks of MPT-FLIM images were taken of treated human skin; gold nanoparticle luminescence signal was quantified using a stringent range of $\alpha_1$% 90–100 to exclude skin autofluorescence. Significantly more gold nanoparticle signal was detected deep in the stratum corneum in the AuNP-TOL group at 4 h ($p<0.001$), but not in the other 4-hour treatment groups (Fig. 6a). Gold nanoparticle luminescence signals were found within the stratum corneum in both gold nanoparticle treatment groups after 24 h treatment, but not in vehicle-only groups (Fig. 6b). Gold nanoparticle luminescence signals were found significantly deeper in the AuNP-TOL-treated group than AuNP-Aq group at 24 h ($p<0.05$), supporting the histological findings above. Intensity of gold aggregate reflectance signal in furrows was quantified from RCM analysis (Fig. 6c). These data show the presence of

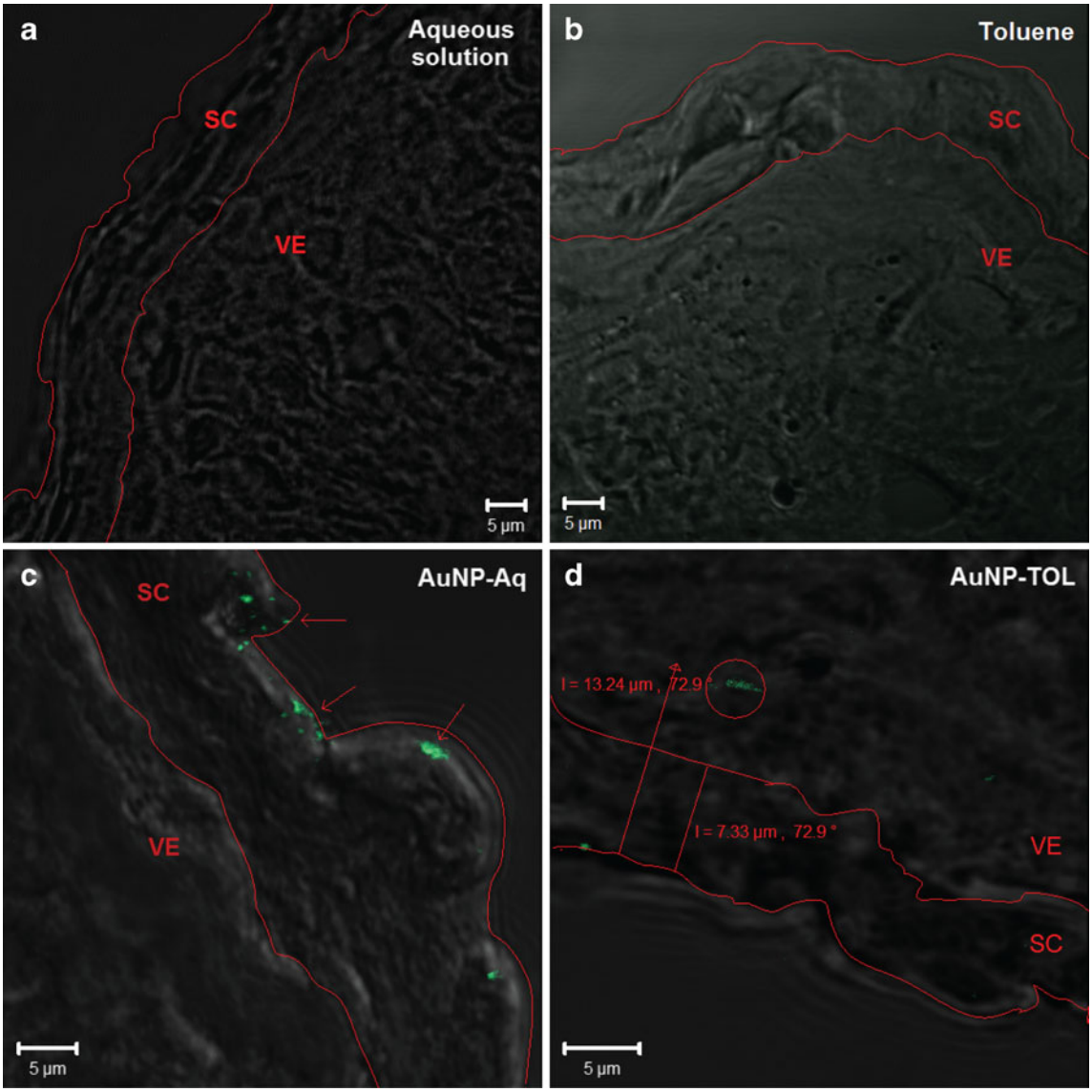


**Fig. 4** MPT of thawed skin treated for 24 h. (**a**–**d**) 10 $\mu$m-thick cryosectioned skin from aqueous, toluene, AuNP-Aq, and AuNP-TOL groups. The images are overlays of light transmission and gold luminescence images. The stratum corneum and viable epidermis are labelled SC and VE; the SC is outlined in red. The red arrows indicate AuNP in the AuNP-Aq image and the circle indicates AuNP in the AuNP-TOL image that is 13 $\mu$m deep.

significantly more highly reflective aggregates deep within the furrows of AuNP-Aq-treated skin ($p<0.0001$), compared to all other groups.

## MPT-FLIM Analysis of NAD(P)H at 4 and 24 Hours Post-Treatment

MPT-FLIM analysis of NAD(P)H was carried out in epidermis of excised human skin. FLIM data were taken via a depth series of *en face* images that were processed to quantify total NAD(P)H intensity and $\alpha_1/\alpha_2$ ratio. The $\alpha_1/\alpha_2$ ratio is inversely related to the metabolic rate (35). Toluene-treated skin, including toluene alone and AuNP-TOL, at both 4 and 24 h showed low NAD(P)H signals similar to those seen in non-viable skin (Fig. 2j, n, l, p; Fig. 7a, b) (36). Total NAD(P)H signal in toluene-treated groups was significantly depressed when compared to the aqueous groups, $p<0.001$. After 4-hour treatment with AuNP-Aq, total NAD(P)H levels were significantly lower than aqueous-only controls, $p<0.01$. $\alpha_1/\alpha_2$ data mirrored the total NAD(P)H results with a significant increase in the ratio of toluene-treated groups compared to the aqueous groups ($p<0.001$) (Fig. 7c, d). At 24-hour treatment, differences in $\alpha_1/\alpha_2$ ratio were less pronounced than in total NAD(P)H analysis. This may be due to natural skin necrosis after removal from the donor, as we have previously reported (36). Unlike the total NAD(P)H data, the $\alpha_1/\alpha_2$ ratio data showed no differences between the aqueous groups.

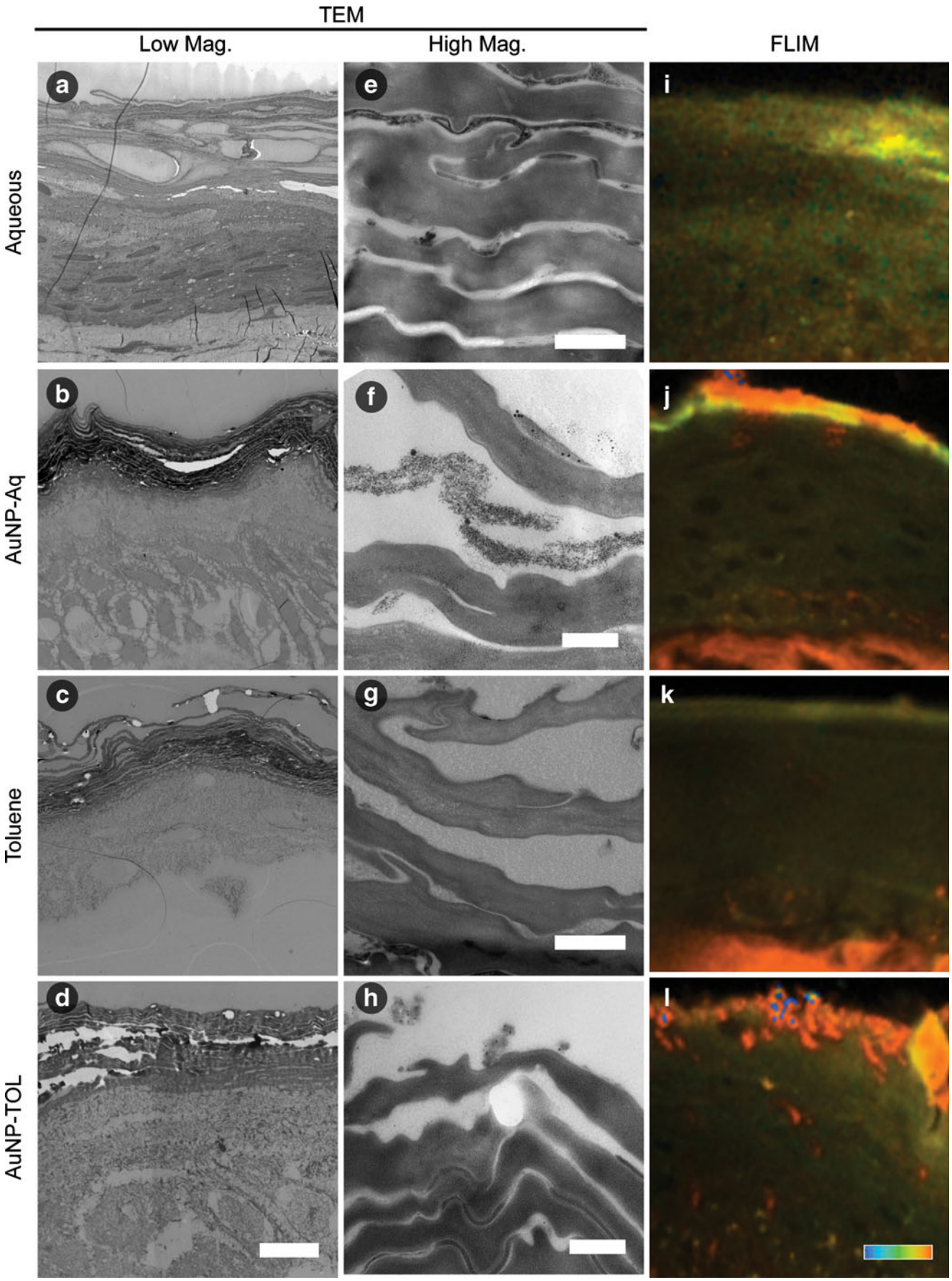
TEM
Low Mag.
High Mag.
FLIM
Aqueous
AuNP-Aq
Toluene
AuNP-TOL
a
b
c
d
e
f
g
h
i
j
k
l

◀ **Fig. 5** Gold nanoparticle penetration in cross-sections using TEM and MPT-FLIM. Low and high magnification images of the epidermis and superficial stratum corneum from each of the treatment groups (**a**–**h**). Scale bars: 1 μm (**a**–**d**); 200 nm (**e**, **f**); 500 nm (**g**, **h**). Pseudocolored MPT-FLIM images (**i**–**l**) show the penetration pattern of gold nanoparticles (orange to red). MPT-FLIM imaging with a 740 nm excitation wavelength and emission was filtered with a 350-650 nm band pass filter (BG39). (**i**–**l**) Scale bar: 50 μm; pseudocolored MPT-FLIM images are $\alpha_1$% 50–100 from blue to red.

## DISCUSSION

Nanoparticle skin penetration is a multi-factorial and multi-step process that is affected by a number of factors, including the skin type, barrier damage, and inherent physicochemical attributes (size, shape, surface charge, etc.) and vehicle of the applied colloids. Measuring nanoparticle penetration and NAD(P)H effects in excised human skin was the focus of this microscopy study. Human skin was chosen, being regarded as the "gold standard" and most reliable set-up for *in vitro* skin penetration studies, especially in human dermal risk assessment (37). The public could come in contact with nanoparticles non-intentionally in daily life via handling of several products such as cleaning agents, sport clothes, paints, etc., in addition to environmental exposure to water and air contaminated with nanoparticles. Last but not least, the safety of personnel working in industry and research handling nanoparticles was not in focus. Though nanotechnology is finding a lot of applications in pharmaceutical industry, safety issues should be further studied, highlighting the importance of this study. Aside from occupational health issues, studying the behavior of nanoparticles with the skin barrier is a very important basic research approach for later application in designing topical drug delivery systems with optimal parameters. This is especially true when solvents like terpenes are used in topical formulations (38). Our experimental design was congruent with previous gold nanoparticle skin penetration studies with similar exposure times and use of static Franz cells. Our study design was unique because we evaluated viable human skin and utilised clinical dermoscopy, RCM and MPT-FLIM. Therefore, our results can be directly compared to future clinical studies because our assessment technologies can be applied *in vivo*.

Sonavane *et al.* (2008) showed that 15-nm gold nanoparticles in aqueous solution were capable of penetrating through full thickness rat skin over 24 h using spectrophotometry and TEM (39). Similarly, Larese Filon *et al.* (2011) showed that aqueous 12.9-nm gold nanoparticles could penetrate completely through thawed human skin over

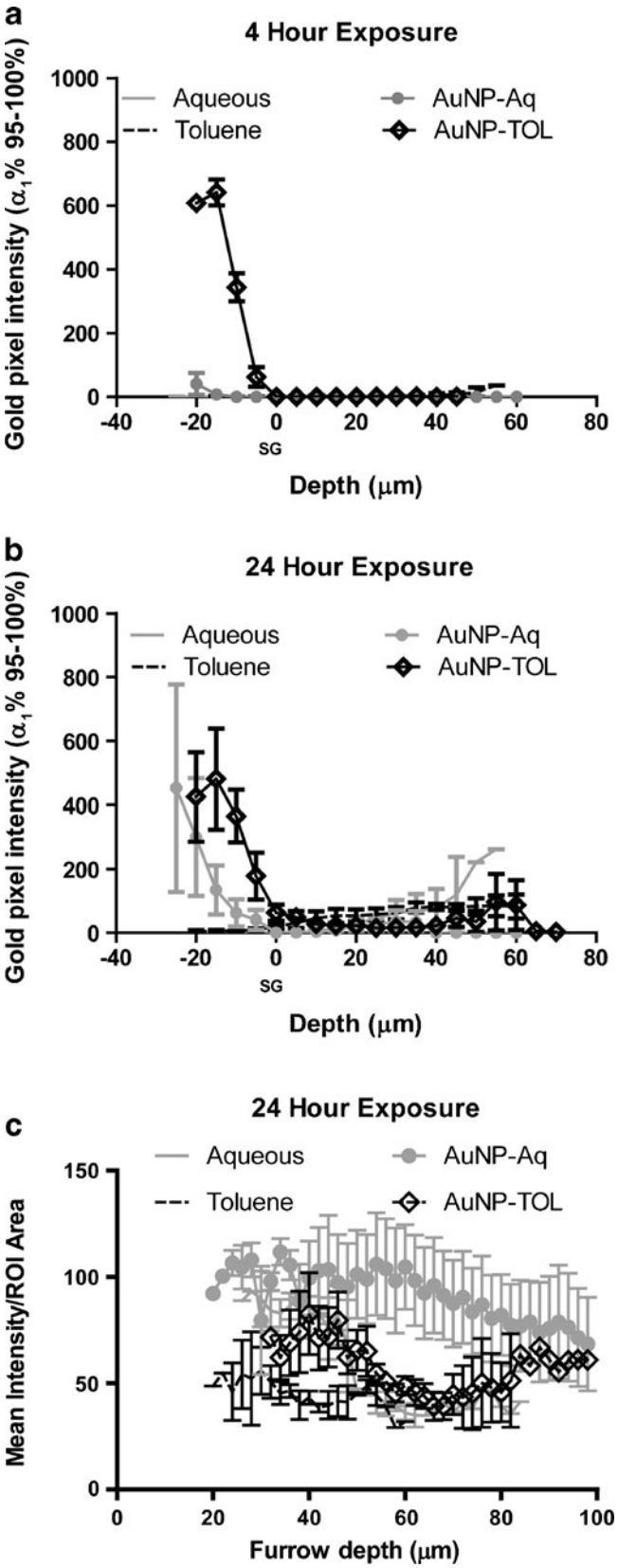


**Fig. 6** Gold nanoparticle luminescence and reflectance skin profiles. Data ▶ from MPT-FLIM depth series (SG indicates the stratum granulosum) were processed to identify gold nanoparticle luminescence intensity as a function of depth in non-furrow-containing regions. Data are shown for both 4 and 24 h treatment groups (**a**, **b**). Furrow reflectance intensity was derived from the stratum corneum and outer surface of furrow areas; the top of the skin is at 0 μm (**c**). These data were gathered from a depth series of *en face* images.

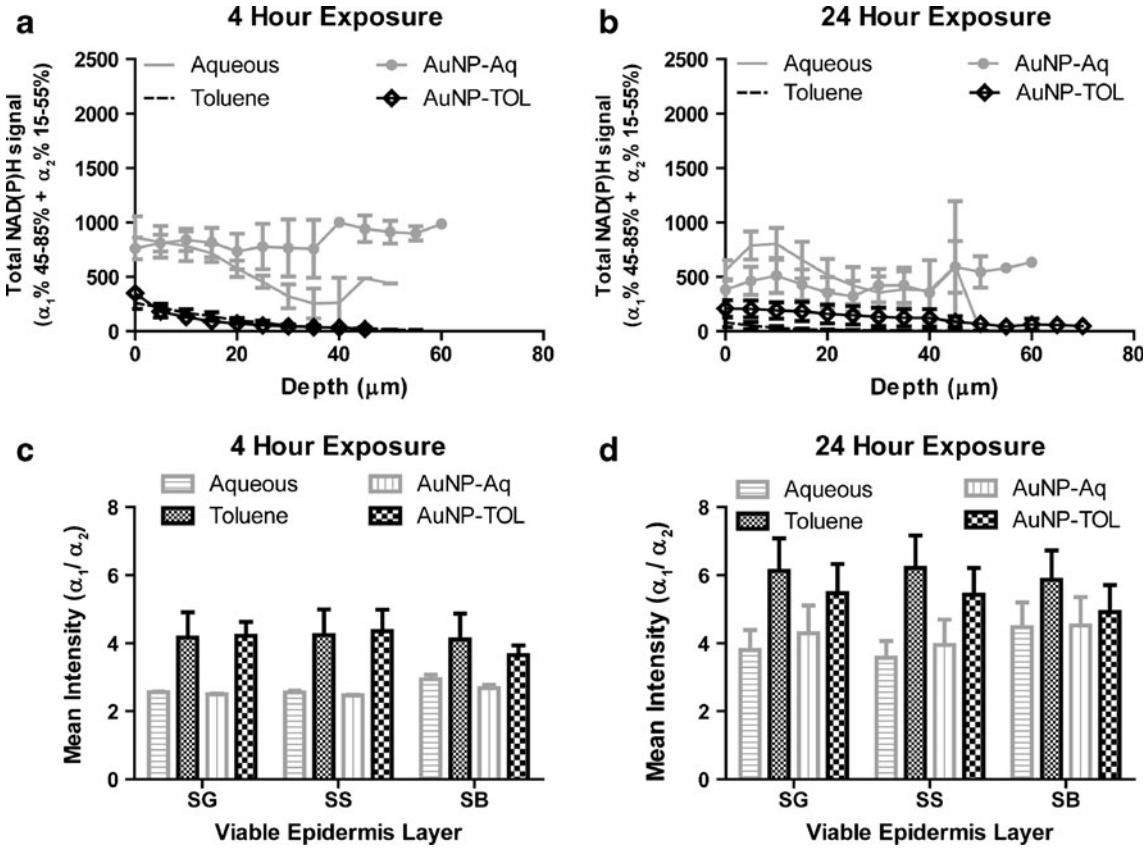


**Fig. 7** NAD(P)H effects from MTP-FLIM imaging. NAD(P)H signals were separated from gold nanoparticle luminescence by selecting $\alpha_1$% 45–85. NAD(P)H intensity with depth in non-furrow areas (SG, SS, and SB) from skin treated for 4 and 24 h (**a**, **b**). The $\alpha_1/\alpha_2$ ratio is inversely related to the metabolic rate and was calculated for each of the treatment groups at 4 and 24 h.

24 h using ICP to detect gold ions in the receptor (29). Our study showed penetration into stratum corneum but not beyond using 14.9-nm gold nanoparticles in aqueous solution with TEM, MPT-FLIM, and RCM. This incongruity with the rat skin study by Sonovane *et al.* and thawed human skin by Larese Filon *et al.* might be due to the type of skin used. Viable rat skin is thinner and more permeable to nanoparticles than viable human skin (7,40). Thawed human skin is non-viable (36) and, therefore, is likely to be more permeable to nanoparticles than viable human skin. The use of MPT-FLIM to detect luminescent nanoparticles eliminates the possibility of solubilised nanoparticle residues from our analysis because luminescence only occurs in the presence of the intact particle, thus eliminating potentially confounding factors like soluble or endogenous ions, as can occur with ICP analysis. The inability of the 15-nm AuNP-Aq to cross skin barrier could be also attributed to their surface aggregation, as observed by dermoscopy. This could be attributed to the exchange of the citrate ions on the gold nanoparticle surface with skin proteins or lipids, as shown in other biological environments (41,42).

There were substantial similarities between our results with nanoparticles in toluene and the study by Xia *et al.* (2010) (17). They showed increased nanoparticle penetration in the presence of solvents that included toluene. As pig skin is more similar to human skin and this study was done *in vivo* using Yorkshire weanling pigs, it is a more relevant comparison to our study than rat skin or thawed human skin. The expected similarities in nanoparticle penetration between human and porcine skin are based on similar solute fluxes previously observed (43,44).

Our TEM data showed widespread disruption of the epidermal ultrastructure in toluene-treated samples. These TEM images showed discontinuous cell membranes and particulates throughout the samples that were not present in aqueous-treated groups. Disruption of lipid barriers by toluene could have directly led to the increased nanoparticle penetration we observed in the AuNP-TOL-treated skin. We observed dramatic decreases in total NAD(P)H autofluorescence with toluene treatment. These data were similar to those from necrotic skin we previously published (36). Therefore, we hypothesize that toluene-treated skin was metabolically disrupted within 4 h of treatment by chemically induced necrosis. TEWL measurements indicate the integrity of the skin specimens with general increase in values after

24 h of occlusive conditions due to over-hydration of the skin. Regarding nanoparticle penetration only, long-term incubation revealed some penetration, indicating that skin barrier was not completely disrupted. Skin treated with gold nanoparticles in aqueous solution revealed lower total NAD(P)H signal, but metabolic rate appeared unchanged. We have observed decreases in the metabolic rate of silver nanoparticle-treated human skin (7), so we hypothesize that the unchanged metabolic rate data from gold nanoparticle treatments suggest that the total NAD(P)H signal may have been reduced by gold nanoparticle light scattering and not metabolic effects.

## CONCLUSION

Our data showed that 15-nm gold nanoparticles in aqueous solution tended to aggregate on the superficial stratum corneum after 24 h exposure, while 6-nm gold nanoparticles in toluene penetrated through stratum corneum and into epidermal layers of human skin. Our NAD(P)H imaging data showed that epidermis was not viable at 4 and 24 h post-toluene treatment regardless of the presence of gold nanoparticles. Nevertheless, an exclusive role of the size or solvent on skin penetration should not be the conclusion of this research work. A more in-depth study of the single size and solvent effects is therefore in need. The results of this paper, however, should raise public awareness regarding the environmental exposure to nanoparticles, especially for personnel in research and industry. In the future, similar studies are needed characterizing the impact of different physicochemical properties of nanoparticles with regard to penetration and metabolic effect on the skin.

## ACKNOWLEDGMENTS & DISCLOSURES

The authors HIL, LK, and MS thank the Ministry of Higher Education and Scientific Research, Egypt, and DAAD for financial support, as well as Karl-Heinz Kostka (Department of Plastic and Hand Surgery, Caritaskrankenhaus, Lebach, Germany) for providing human skin employed in our study and Leon Muijs for preparing cross-sections of thawed skin samples. TEM images of individual AuNP dispersions were generated by Nico Reum. Australian National Health and Medical Research Council funded this research (ID# 569694).

## REFERENCES

1. Mooradia A. Photoluminescence of metals. Phys Rev Lett. 1969;22:185.
2. Prow TW, Chen X, Prow NA, Fernando GJ, Tan CS, Raphael AP, *et al.* Nanopatch-targeted skin vaccination against West Nile Virus and Chikungunya virus in mice. Small. 2010;6:1776–84.
3. Schneider M, Stracke F, Hansen S, Schaefer UF. Nanoparticles and their interactions with the dermal barrier. Dermatoendocrinol. 2009;1:197–206.
4. On regulatory aspects of nanomaterials. http://ec.europa.eu/health/ph_risk/commithttp://www.schneiderchildrenshospital.org/peds_html_fixed/peds/derm/burns.htmtees/04_sccp/docs/sccp_o_123.pdf (accessed 15/09/2010).
5. Robertson TA, Sanchez WY, Roberts MS. Are commercially available nanoparticles safe when applied to the skin? J Biomed Nanotechnol. 2010;6:452–68.
6. Monteiro-Riviere NA, Tran CL. Nanotoxicology: characterization, dosing and health effects. New York: Informa Healthcare; 2007.
7. Prow TW, Grice JE, Lin LL, Faye R, Butler M, Becker W, *et al.* Nanoparticles and microparticles for skin drug delivery. Adv Drug Deliv Rev. 2011.
8. Küchler S, Abdel-Mottaleb M, Lamprecht A, Radowski MR, Haag R, Schäfer-Korting M. Influence of nanocarrier type and size on skin delivery of hydrophilic agents. Int J Pharm. 2009;377:169–72.
9. Rouse JG, Yang J, Ryman-Rasmussen JP, Barron AR, Monteiro-Riviere NA. Effects of mechanical flexion on the penetration of fullerene amino acid-derivatized peptide nanoparticles through skin. Nano Lett. 2007;7:155–60.
10. Mortensen LJ, Oberdorster G, Pentland AP, Delouise LA. *In vivo* skin penetration of quantum dot nanoparticles in the murine model: the effect of UVR. Nano Lett. 2008;8:2779–87.
11. Paliwal S, Menon GK, Mitragotri S. Low-frequency sonophoresis: ultrastructural basis for stratum corneum permeability assessed using quantum dots. J Invest Dermatol. 2006;126:1095–101.
12. Coulman SA, Anstey A, Gateley C, Morrissey A, McLoughlin P, Allender C, *et al.* Microneedle mediated delivery of nanoparticles into human skin. Int J Pharm. 2009;366:190–200.
13. Crosera M, Bovenzi M, Maina G, Adami G, Zanette C, Florio C, *et al.* Nanoparticle dermal absorption and toxicity: a review of the literature. Int Arch Occup Environ Health. 2009;82:1043–55.
14. Cevc G, Vierl U. Nanotechnology and the transdermal route: a state of the art review and critical appraisal. J Contr Release. 2010;141:277–99.
15. Prow TW, Grice JE, Lin LL, Faye R, Butler M, Becker W, *et al.* Nanoparticles and microparticles for skin drug delivery. Adv Drug Deliv Rev. 2011;63:470–91.
16. Roberts MS, Dancik Y, Prow TW, Thorling CA, Lin LL, Grice JE, *et al.* Non-invasive imaging of skin physiology and percutaneous penetration using fluorescence spectral and lifetime imaging with multiphoton and confocal microscopy. Eur J Pharm Biopharm. 2011;77:469–88.
17. Xia XR, Monteiro-Riviere NA, Riviere JE. Skin penetration and kinetics of pristine fullerenes (C60) topically exposed in industrial organic solvents. Toxicol Appl Pharmacol. 2010;242:29–37.
18. Harper M. Assessing workplace chemical exposures: the role of exposure monitoring. J Environ Monit. 2004;6:404–12.
19. Hoover MD, Stefaniak AB, Day GA, Geraci CL. Exposure assessment considerations for nanoparticles in the workplace. In: Monteiro-Rivieread NA, Tran CL, editors. Nanotoxicology: characterization, dosing and health effects. New York: Informa Healthcare; 2007. p. 71–83.
20. Rivieread JE, Brooks JD. Predicting skin permeability from complex chemical mixtures: dependency of quantitative structure permeation relationships on biology of skin model used. Toxicol Sci. 2011;119:224–32.
21. Rivieread JE, Brooks JD. Predicting skin permeability from complex chemical mixtures. Toxicol Appl Pharmacol. 2005;208:99–110.

22. Xia XR, Monteiro-Riviere NA, Riviere JE. Intrinsic biological property of colloidal fullerene nanoparticles (nC60): lack of lethality after high dose exposure to human epidermal and bacterial cells. Toxicol Lett. 2010;197:128–34.
23. Farrer RA, Butterfield FL, Chen VW, Fourkas JT. Highly efficient multiphoton-absorption-induced luminescence from gold nanoparticles. Nano Lett. 2005;5:1139–42.
24. Labouta HI, Kraus T, El-Khordagui LK, Schneider M. Combined multiphoton imaging-pixel analysis for semiquantitation of skin penetration of gold nanoparticles. Int J Pharmaceut. 2011;413:279–82.
25. Boyd GT, Yu ZH, Shen YR. Photoinduced Luminescence from the Noble-Metals and Its Enhancement on Roughened Surfaces. Phys Rev B. 1986;33:7923–36.
26. Yang Y, Qu Y, Lu X. Global gene expression analysis of the effects of gold nanoparticles on human dermal fibroblasts. J Biomed Nanotechnol. 2010;6:234–46.
27. Schaeublin NM, Braydich-Stolle LK, Schrand AM, Miller JM, Hutchison J, Schlager JJ, *et al.* Surface charge of gold nanoparticles mediates mechanism of toxicity. Nanoscale. 2011; 3:410–20.
28. Lu S, Xia D, Huang G, Jing H, Wang Y, Gu H. Concentration effect of gold nanoparticles on proliferation of keratinocytes. Colloids Surf B Biointerfaces. 2010;81:406–11.
29. Larese Filon F, Crosera M, Adami G, Bovenzi M, Rossi F, Maina G. Human skin penetration of gold nanoparticles through intact and damaged skin. Nanotoxicology. 2011. doi:10.3109/17435390.2010.551428.
30. Turkevich J, Stevenson PC, Hillier J. A study of the nucleation and growth processes in the synthesis of colloidal gold. discuss, Faraday Soc. 1951;55–57.
31. Zheng N, Fan J, Stucky GD. One-step one-phase synthesis of monodisperse noble-metallic nanoparticles and their colloidal crystals. J Am Chem Soc. 2006;128:6550–1.
32. Wagner H, Kostka KH, Adelhardt W, Schaefer UF. Effects of various vehicles on the penetration of flufenamic acid into human skin. Eur J Pharm Biopharm. 2004;58:121–9.
33. Lin LL, Grice JE, Butler MK, Zvyagin AV, Becker W, Robertson TA, *et al.* Time-Correlated Single Photon Counting for Simultaneous Monitoring of Zinz Oxide Nanoparticles and NAD(P)H in Intact and Barrier Disrupted Volunteer Skin. Pharm Res. 2011. doi:10.1007/s11095-011-0515-5.
34. Schneider G, Decher G. Functional core/shell nanoparticles via layer-by-layer assembly. Investigation of the experimental parameters for controlling particle aggregation and for enhancing dispersion stability. Langmuir. 2008;24:1778–89.
35. Bird DK, Yan L, Vrotsos KM, Eliceiri KW, Vaughan EM, Keely PJ, *et al.* Metabolic mapping of MCF10A human breast cells via multiphoton fluorescence lifetime imaging of the coenzyme NADH. Cancer Res. 2005;65:8766–73.
36. Sanchez WY, Prow TW, Sanchez WH, Grice JE, Roberts MS. Analysis of the metabolic deterioration of *ex vivo* skin from ischemic necrosis through the imaging of intracellular NAD(P)H by multiphoton tomography and fluorescence lifetime imaging microscopy. J Biomed Opt. 2010;15:046008.
37. Godinand B, Touitou E. Transdermal skin delivery: predictions for humans from *in vivo*, *ex vivo* and animal models. Adv Drug Deliv Rev. 2007;59:1152–61.
38. Okyar A, Nuriyev M, Yildiz A, Pala-Kara Z, Ozturk N, Kaptan E. The effect of terpenes on percutaneous absorption of tiaprofenic acid gel. Arch Pharm Res. 2010;33:1781–8.
39. Sonavane G, Tomoda K, Sano A, Ohshima H, Terada H, Makino K. *In vitro* permeation of gold nanoparticles through rat skin and rat intestine: effect of particle size. Colloid Surface B. 2008;65:1–10.
40. Prow TW, Monteiro-Riviere NA, Inman AO, Grice JE, Chen X, Zhao X, *et al.* Quantum dot penetration into viable human skin. Nanotoxicology. 2011.
41. Parfenov AS, Salnikov V, Lederer WJ, Lukyanenko V. Aqueous diffusion pathways as a part of the ventricular cell ultrastructure. Biophys J. 2006;90:1107–19.
42. Lacerda SH, Park JJ, Meuse C, Pristinski D, Becker ML, Karim A, *et al.* Interaction of gold nanoparticles with common human blood proteins. ACS Nano. 2010;4:365–79.
43. Westerand RC, Maibach HI. Percutaneous absorption of topical corticosteroids. Curr Probl Dermatol. 1993;21:45–60.
44. Wester RC, Melendres J, Sedik L, Maibach H, Riviere JE. Percutaneous absorption of salicylic acid, theophylline, 2, 4-dimethylamine, diethyl hexyl phthalic acid, and p-aminobenzoic acid in the isolated perfused porcine skin flap compared to man *in vivo*. Toxicol Appl Pharmacol. 1998;151:159–65.